Sources of carbon to suspended particulate organic matter in the northern Gulf of Mexico

Rogers, Kelsey L.; Bosman, Samantha H.; Weber, Sarah; Magen, Cedric; Montoya, Joseph P.; Chanton, Jeffrey P.

ELEMENTA
Science of the Anthropocene

RESEARCH ARTICLE

Sources of carbon to suspended particulate organic matter in the northern Gulf of Mexico

Kelsey L. Rogers[*,†], Samantha H. Bosman[†], Sarah Weber[‡], Cedric Magen[§], Joseph P. Montoya[‖] and Jeffrey P. Chanton[†]

Suspended particulate organic carbon (POC_{susp}) in the Gulf of Mexico is unique compared to other seas and oceans. In addition to surface primary production, isotopic analysis indicates that microbial cycling of oil and riverine inputs are primary sources of carbon to POC_{susp} in the Gulf. To characterize POC_{susp} from seep sites and non-seep north central Gulf (NCG) sites potentially affected by the Deepwater Horizon (DWH) spill, we analyzed 277 and 123 samples for $\delta^{13}C$ and $\Delta^{14}C$ signatures, respectively. Depth, partitioned into euphotic (<300 m) and deep (>300 m), was the main driver of spatial $\delta^{13}C$ differences, with deep depths exhibiting ^{13}C depletion. Both deep depths and proximity to sources of natural seepage resulted in ^{14}C depletion. A two-endmember mixing model based on $\Delta^{14}C$ indicated that sources to POC_{susp} were 14–29% fossil carbon at NCG sites and 19–57% at seep sites, with the balance being modern surface production. A six-component Bayesian mixing model MixSIAR, using both ^{13}C and ^{14}C, suggested that riverine inputs were an important carbon source to POC_{susp} contributing 34–46%. The influence of seeps was localized. Below the euphotic zone at seep sites, 46 ± 5% (n = 9) of the carbon in POC_{susp} was derived from environmentally degraded, transformed oil; away from seeps, transformed oil contributed 15 ± 4% (n = 39). We hypothesized that, at NCG sites removed from hydrocarbon seep sources, isotopic signatures would be depleted following the spill and then shift towards background-like enriched values over time. At deep depths we observed decreasing $\Delta^{14}C$ signatures in POC_{susp} from 2010 to 2012, followed by isotopic enrichment from 2012 to 2014 and a subsequent recovery rate of 159‰ per year, consistent with this hypothesis and with biodegraded material from DWH hydrocarbons contributing to POC_{susp}.

Keywords: Suspended POC; Radiocarbon; Deepwater horizon; Carbon sources

Introduction

The introduction of fossil hydrocarbon-derived material, whether by anthropogenic inputs or natural seepage, provides a unique source of carbon source to the sea. In most areas of the Atlantic and Pacific oceans, surface primary production is the main carbon source to the deep ocean. Typically, only about 1% of the carbon fixed at the surface reaches the deep seafloor. Along the way, most of the organic matter is consumed and degraded, exchanging between the different carbon pools in the water column — dissolved inorganic carbon (DIC), dissolved organic carbon (DOC), and sinking and suspended particulate organic carbon (POC_{sink}, POC_{susp}), before the residual amount finally reaches the seafloor.

Of these pools, POC_{susp} is uniquely capable of providing insights into the sources of carbon to the water column and those fueling the microbial loop. The small particle size and relatively short residence time that characterize POC_{susp} make it more sensitive than other carbon pools to recording variations in inputs. The different carbon pools can be defined operationally by size. The smallest end of this size continuum is DOC, which we define as organic carbon that passes through a filter of 0.7-μm pore size. POC_{susp} is any organic matter collected on the 0.7-μm filter, while POC_{sink} is comprised of those particles typically larger than 50 μm (Deuser, 1986). Due to the small difference in size, DOC and POC_{susp} are more similar to each other chemically than to POC_{sink} (Druffel et al., 1996). As DOC is partially controlled by microbial processes, the DOC-POC_{susp} connection provides a link between microbial processes and the larger particles that can move carbon up the food chain (Chanton et al., 2012; Cherrier et al., 2014). Linkage with the microbial

* Department of Geosciences and Natural Resource Management, University of Copenhagen, Copenhagen, DK

† Department of Earth, Ocean and Atmospheric Science, Florida State University, Tallahassee, Florida, US

‡ Department of Biological Oceanography, Leibniz Institute for Baltic Sea Research Warnemünde, Rostock, DE

§ University of Maryland Center for Environmental Studies, Chesapeake Biological Laboratory, Solomons, Maryland, US

‖ School of Biological Sciences, Georgia Institute of Technology, Atlanta, Georgia, US

Corresponding author: Kelsey L. Rogers (klrogers@ign.ku.dk)

loop has also been observed in the microbial uptake of dissolved inorganic nitrogen and possible methanodi-azotrophy through $\delta^{15}N$ isotope analysis (Montoya et al., 1990; Fernandez et al., 2016).

The residence times of DOC, POC_{sink}, and POC_{susp} range widely, resulting in different degrees of sensitivity of each carbon pool to different inputs. DOC is the second largest carbon reservoir in the ocean, amounting to about 650 Pg of mostly recalcitrant carbon, with a residence time of 1000–6000 years (Williams and Druffel, 1987). The concentrations of POC_{susp} and POC_{sink} in the water are much lower than DOC, but the flux of POC_{sink} through the water column is much greater than POC_{susp}, with a residence time of about a month (Deuser, 1986). POC_{sink} is determined primarily by surface phytoplankton production (Chanton et al., 2018), which draws on the DIC pool, the largest carbon reservoir in the ocean at 38,000 Pg (Hansell and Carlson, 2014). POC_{susp} floats in the water for 5–10 years (Bacon and Anderson, 1982). Its low concentrations in the open ocean, typically from less than 10 μM C in surface waters to about 1 μM C at depths below 500 m (McNichol and Aluwihare, 2007), and short residence times increase the sensitivity of this pool to other carbon sources, although the DOC and POC_{sink} pools have also been observed to reflect variations in carbon input associated with the Gulf of Mexico (GOM) Deepwater Horizon (DWH) spill (Yan et al., 2016; Walker et al., 2017; Chanton et al., 2018; Geiring et al., 2018).

Studies in the late 1980s and early 1990s used stable and radiocarbon isotope analysis of POC to determine sources of oceanic particulates. Druffel et al. (1992, 1996, 2003) analyzed stable and radiocarbon isotopes of particulates from the Sargasso Sea and central North Pacific which indicated that POC_{sink} and POC_{susp} are derived primarily from surface phytoplankton production. POC_{susp} is enriched in radiocarbon from being formed at the surface and becomes more depleted with depth. In the GOM, $\delta^{13}C$ values for surface production range from –20 to –22‰ (Chanton and Lewis, 2002), and, at the time of the oil spill, $\Delta^{14}C$ values for surface production ranged from 39 to 41‰ (Chanton et al., 2012, 2018).

In marginal seas, the sources of POC_{susp} can vary. Bauer et al. (2002) found highly depleted $\delta^{13}C$ and $\Delta^{14}C$ values for POC_{susp} at depth along the Mid-Atlantic Bight (MAB). The radiocarbon depletion near the seafloor of POC_{susp} has been attributed to resuspension of old sediment or organic matter and adsorption of DOC onto POC_{susp} (Druffel et al., 1992, 1996, 2003; Bauer and Druffel, 1998; Bauer et al., 2002). Flocculating particles due to heterotrophic activity could also play a role in depleting $PO^{14}C_{susp}$ (Druffel et al., 1992). Bauer et al. (2002) suggested that deep shelf $PO^{14}C$ from the MAB could be caused by natural hydrocarbon seepage; however, at the time of collection there was no evidence of such seepage, leading Bauer et al. (2002) to conclude that the depletion was due most likely to resuspended sediment. The similar correlation of $\delta^{13}C$ and $\Delta^{14}C$ observed between particulates from the MAB (Bauer et al., 2002) and the Desoto Canyon of the Gulf of Mexico (**Figure 1**) (Cherrier et al., 2014) suggests similar sources of carbon. In 2014, Skarke et al. (2014) reported the discovery of a major hydrocarbon seep field in the same area of the MAB that Bauer et al. (2002) had
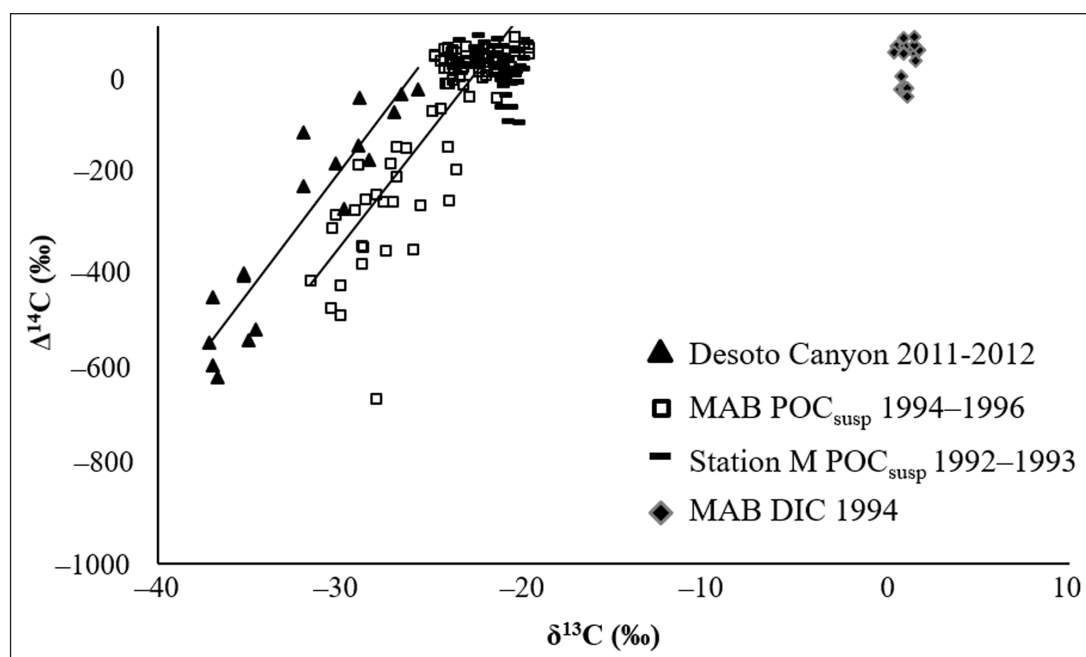

Figure 1: $\delta^{13}C$ and $\Delta^{14}C$ signatures of POC_{susp} and DIC in the ocean. Data for POC_{susp} from Pacific Station M (bold dashes; Druffel et al., 1996) showed no trend, indicating a single source, surface primary production, to the POC_{susp}. The covariation in $\delta^{13}C$ and $\Delta^{14}C$ for POC_{susp} from the Mid-Atlantic Bight (MAB, open squares; Bauer et al., 2001, 2002) and Desoto Canyon in the Gulf of Mexico (solid triangles; Cherrier et al., 2014) indicates the incorporation of another carbon source. Data for DIC from MAB are from Bauer et al. (2001). For data fit to linear regression analysis for Desoto Canyon 2010–2011: y = 49.137x + 1277.5, r = 0.929, n = 18, p < 0.0001; for MAB 2002: y = 47.708x + 1081.4, r = 0.845, n = 106, p < 0.0001. DOI: https://doi.org/10.1525/elementa.389.f1

sampled. The hydrocarbons from this seep field could well be the cause of the correlation between the depleted $\delta^{13}C$ and $\Delta^{14}C$ of POC from the MAB (**Figure 1**).

In April of 2010, the DWH Blowout released 717–789 million liters (4.5–4.9 million barrels) of oil and 500,000 t of gaseous hydrocarbons into the northern central Gulf of Mexico (Lehr et al., 2010; Joye et al., 2011). An estimated 30% of the released hydrocarbons formed a deep-water hydrocarbon plume between 1000-m and 1200-m depths (Valentine et al., 2010; Ryerson et al., 2012). The bulk of the gaseous hydrocarbons were primarily methane (Joye et al., 2011), but less than 0.01% of the gases reached the surface (Kessler et al., 2011; Yvon-Lewis et al., 2011). Crespo-Medina et al. (2014) measured methane oxidation rates in the water column following the DWH event. At the depth of the deep-water hydrocarbon plume, concentrations of methane and the gene methane monooxygenase (*pmoA*) were elevated, as were methane-oxidation rates. Cherrier et al. (2014) presented evidence that this DWH-derived CH_4 was found in the POC_{susp} of the Gulf in 2011–2012 (**Figure 1**). Assimilation of methane by methanotrophs has been found to be very efficient in other systems, e.g., converting 63–85% of methane into biomass at landfill sites (Börjesson et al., 1998, 2001). Du and Kessler (2012) estimated, using theoretical calculations of oxygen usage from the dissolved oxygen anomaly present in the deep-water hydrocarbon plume, that hydrocarbon degradation generated 0.36 ± 0.11 mg biomass per mg hydrocarbon. They also estimated that 0.10 ± 0.11 Tg of hydrocarbons, primarily methane, were converted into microbial biomass within the deep-water hydrocarbon plume. This biomass, including after cell senescence and viral lysis, would be an input to the POC_{susp} pool.

Methane can also be generated microbially in the oceanic water column under aerobic conditions (Karl et al., 2008). This process occurs in the Gulf of Mexico (Rakowski et al., 2015), as evidenced by CH_4 concentrations and relative microbial abundances co-varying significantly from the seafloor to the euphotic zone. Thus, our characterization of the sources contributing to POC_{susp} included characterizing the isotopic composition of biogenically produced methane.

Several studies following the DWH event analyzed POC and plankton in the GOM, finding depleted $\delta^{13}C$ and $\Delta^{14}C$ signatures (Graham et al., 2010; Chanton et al., 2012; Cherrier et al., 2014). Chanton et al. (2012) and Cherrier et al. (2014) found a linear relationship between $\delta^{13}C$ and $\Delta^{14}C$ signatures, from modern photosynthetic production to a hydrocarbon endmember, with both the plankton and POC falling along the line, indicating the incorporation of material originally sourced from hydrocarbons, as well as the movement of this material up the food web (Wilson et al., 2016).

The purpose of this study was to characterize $\delta^{13}C$ and $\Delta^{14}C$ signatures of POC_{susp} in the GOM following the oil spill and as the system recovered from it, determining a new post-spill baseline for $\delta^{13}C$ and $\Delta^{14}C$ signatures of POC_{susp} in the GOM in the process. (For parallel work on POC_{sink}, see Chanton et al., 2018.) In the Atlantic and Pacific Ocean basins, the baseline derives from a single dominant source, modern photosynthetic production. No other carbon source contributes more depleted ^{13}C or ^{14}C to the pool of POC_{susp}, so that co-variation between the isotopes (as in **Figure 1**) is not observed. In the GOM, however, the presence of two distinct carbon sources, one associated at times with anthropogenic activity, drives the depletion of both $\delta^{13}C$ and $\Delta^{14}C$ of POC, resulting in the co-variations depicted in **Figure 1**. The continuous input of hydrocarbon-derived material, petrocarbon, from natural seeps could also cause baseline signatures of the GOM to be more depleted than those from the Atlantic or Pacific oceans where input of hydrocarbon-derived material is quantitatively unimportant.

In this study we pursued three goals. First, we tested the hypothesis that, at sites with one-time (DWH) inputs of petrocarbon derived from methane and oil, initial depletion of the carbon isotopic signatures of POC_{susp} would be followed by recovery, shifting the depleted values observed by Cherrier et al. (2014) towards more enriched baseline-like signatures. Assessing baseline signatures of POC_{susp} in the Gulf prior to the DWH spill in 2010 has been difficult, as no $PO^{14}C$ data were collected in the GOM prior to that time. Second, we addressed the question, to what extent are the carbon isotopic values of POC_{susp} in the GOM affected by the seep sites that provide a continuous source of hydrocarbon-derived material to the Gulf as opposed to the one-time input from the DWH? Third, we aimed to determine the relative importance of modern surface marine production and riverine inputs to the different carbon sources in the Gulf, as reflected in POC_{susp}. In this study, we analyzed the stable carbon and radiocarbon isotopes of POC_{susp} collected from across the northern GOM to determine the carbon sources to these particulates. For sources we considered surface marine primary production, riverine input, sediment, two sources of biodegraded methane, and biodegraded oil.

Material and Methods
Sampling and sample preparation
POC_{susp} samples were collected during fourteen cruises over six years from 2010 to 2017 (except 2011), from a total of 43 separate sites across the northern Gulf of Mexico (**Figure 2**). At the time of collection, sites were classified as seep or non-seep, with seep samples collected directly over areas of seafloor seepage, while non-seep samples (designated north central Gulf, NCG) were collected in areas not directly influenced by natural seepage. These determinations were based on map data from MacDonald et al. (2015) and shipboard acoustics used to detect hard bottoms or bubbly streams indicative of a seep site. Over the course of sampling we collected particles from 13 seep and 30 NCG sites.

Water column samples were collected by CTD-Rosette, filtering 1–20 L of water through pre-combusted 47-µm 0.7 GF/F borosilicate filters in plastic housings under gentle pressure filtration (5–10 psi). Filters were stored frozen in combusted aluminum foil and brought back to the lab for acidification in a filter housing unit with dilute (1N) HCl (Fernández-Carrera et al. 2016). Stable carbon isotope ratios of POC_{susp} were analyzed on subsections of the filters using a Carlo-Erba elemental analyzer connected to a Finnegan MAT delta Plus XP Stable Isotope
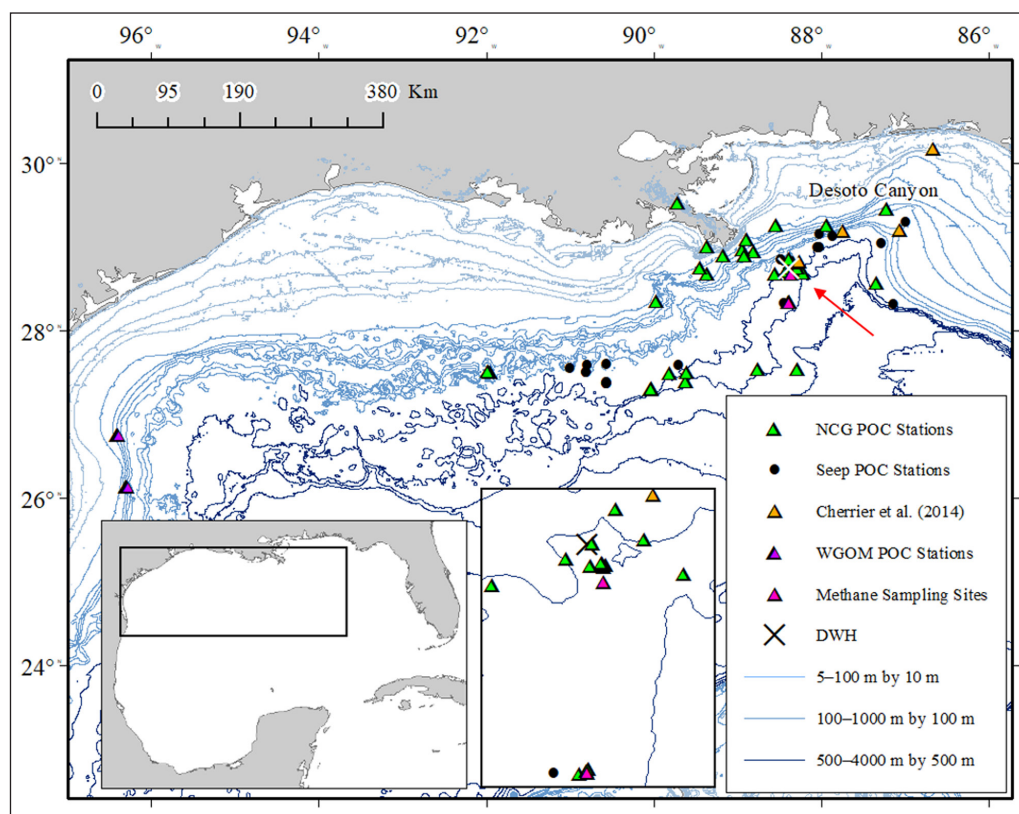
Figure 2: POC$_{susp}$ collection stations in the north central Gulf of Mexico during 2010−2017. The Deepwater Horizon (DWH) site is indicated by a white X in the upper right of the main map and emphasized by a red arrow. North central Gulf (NCG) sites are indicated by green triangles; seep stations, by black circles; western GOM (WGOM) sites, by purple triangles. Data from Cherrier et al. (2014) in the Desoto Canyon are indicated by orange triangles. Sampling sites for biogenic methane in the water column are indicated by pink triangles. The inset map shows an enlarged view of the DWH site (black X) and surrounding sampling sites. The southern biogenic methane sampling site (pink triangle) was approximately 5,900 m east of a seep site. DOI: https://doi.org/10.1525/elementa.389.f2

Ratio Mass Spectrometer (EA-IRMS) at the National High Magnetic Field Laboratory. The results were converted into $\delta^{13}C$ with respect to VPDB (Vienna Pee Dee Belemnite). Samples analyzed after 2014 had a small split, about 10% of the total sample, of CO_2 removed prior to graphitization to be analyzed for $\delta^{13}C$. After $\delta^{13}C$ analysis, the remaining filter was combusted, and the resultant CO_2 was purified cryogenically using the methods of Peterson et al. (1994). The purified CO_2 was flame-sealed in a 6-mm ampule and sent to Woods Hole National Ocean Sciences Accelerator Mass Spectrometry (NOSAMS), University of Georgia Center for Applied Isotope Studies (UGA) or Lawrence Livermore National Laboratory Center for Acceleration Mass Spectrometry (LLNL CAMS) for analysis of natural abundance of radiocarbon. The radiocarbon signatures are reported in the $\Delta^{14}C$ notation as described in Stuiver and Pollach (1977). The blank correction as described in Fernández-Carrera et al. (2016) was applied to both $\delta^{13}C$ and $\Delta^{14}C$ values. Forty coal samples, representing fossil ^{14}C dead carbon, were run to access our procedural blank over the course of this study. The average $\Delta^{14}C$ value was −995 ± 7‰. We also ran 25 azalea leaf standards collected in Tallahassee, Florida, in 2013. The average $\Delta^{14}C$ value was 31 ± 8‰. There was no variation between AMS labs in these samples or the coal blanks.

To estimate the DOC blank adsorbed onto the filters, we attached a second GF/F filter below the filter collecting the POC$_{susp}$. The top filter would collect the POC, leaving the second filter to adsorb only DOC (if that were occurring). From this process, we estimated the DOC blank on the filters to be 0.12 μmoles CO_2, representing 0.3 to 2% of the amount of carbon on the filters.

For water-column CH_4 and its $\delta^{13}C$ isotopic composition, water samples were collected by CTD-Rosette and dispersed to glass bottles in June and July of 2013 at two sites in the northern GOM at 28.669°N; 88.3584°W, and at 28.32554°N and 88.3865°W (**Figure 2**). Methane concentrations were determined by the methods detailed in Magen et al. (2014). The stable isotopic composition of water-column methane was determined from 4-L bottles preserved with KOH as described in Magen et al. (2014). A headspace was introduced into the bottles and flushed into cryogenic trapping system, cryo-focused and run on a Thermo Finnegan Delta V Isotope Ratio Mass Spectrometer at Florida State University. The results were converted into $\delta^{13}C$ with respect to VPDB (Vienna Pee Dee Belemnite).

Temporal trends in non-seep site data
The weighted average of the NCG POC$_{susp}$ per collection year for both $\Delta^{14}C$ and $\delta^{13}C$ was calculated to estimate the inventory of carbon and their isotopic signatures in the water column. The weighted average of radiocarbon was calculated by multiplying the total μmoles CO_2 sent for radiocarbon analysis for each year by the individual

sample size of µmoles CO_2. This proportion was then multiplied by the $\Delta^{14}C$ for each sample and summed for the overall weighted average for that year. For the $\delta^{13}C$ samples, the value for mg C per subsample used for $\delta^{13}C$ analysis was calculated from the regression of the %C and $\delta^{13}C$ of known standards. This value was extrapolated to the whole filter, assuming the sample was spread evenly. The value for total mg C for each sample was converted to µmoles and then summed following the radiocarbon method above.

Mixing models

A two-endmember mixing model based on $\Delta^{14}C$ was used to estimate the percent carbon incorporated from photosynthesis and from all petrocarbon sources, combining methane and oil. The following equation was used to determine the percent carbon from modern surface production, with the denominator equaling the total range of radiocarbon from 39‰ (for marine production; Chanton et al., 2018) to −1000‰:

$$\%_{modern} = \left(\left[1000 + \Delta^{14}C_{POC} \right] / 1039 \right) * 100$$

The percent from hydrocarbons is $100 - \%_{modern}$. We completed a sensitivity test for the two-endmember model by adjusting the total range of $\Delta^{14}C$ by the standard deviation of the modern endmember. The $\Delta^{14}C$ of the modern endmember was the average GOM plankton value from Chanton et al. (2018), 39 ± 26‰ (n = 79).

In addition to the two-endmember mixing model we also employed the Bayesian mixing model MixSIAR Version 3.1 (Stock and Semmens, 2016) to determine the contribution from other potential sources of organic carbon in the GOM. This R version uses probabilities from a Bayesian method to estimate the percent contribution from multiple sources. Using $\Delta^{14}C$ and $\delta^{13}C$ as our tracers, we assumed no fractionation between the sources and the isotopic signatures of the POC. We report the contribution of each source at the mean, including the standard deviation, resulting after 3×10^6 iterations. Our model

was run nesting depth within site type, including the residual * process errors with uninformative priors. Our carbon sources included (mean ± standard deviation [S.D.] for $\Delta^{14}C$ and $\delta^{13}C$, respectively) surface productivity (38.8 ± 25.8‰, and −21 ± 2‰; Chanton et al., 2012, 2018), riverine organic carbon (−154 ± 68‰ and −26 ± 1‰; Cai et al., 2015), sedimentary organic carbon (−200 ± 29‰, and −22 ± 1‰; Chanton et al., 2015), biogenic methane in the water column (38.8 ± 25.8‰, n = 79, and −41 ± 1‰, n = 19; this study), as well as DWH methane ($\Delta^{14}C =$ −1000‰ and $\delta^{13}C =$ −57.4‰; Crespo-Medina et al., 2014) and Macondo oil ($\Delta^{14}C =$ −1000‰ and −27‰; Graham et al., 2010).

Statistics

Statistics were performed using R 3.1.3 R Core Team (2015). The data were not normally distributed, as indicated by the results of Levene's test. Therefore, the non-parametric Mann-Whitney U Test was used to compare the different groups for both $\delta^{13}C$ and $\Delta^{14}C$. We continued the designation of seep versus NCG (non-seep, north-central Gulf) and divided our samples further into two depth categories (euphotic <300 m and deep water >300 m). The four categories we examined were as follows: seep euphotic, seep deep, NCG euphotic, and NCG deep. We used the adjusted p-value of 0.008 to indicate significance, accounting for the multiple comparisons ($\alpha = 0.05$, 6 comparisons). From the z value we calculated the effect size:

$$r = \frac{z}{\sqrt{N}}$$

where r is the effect size, z is the z score, and N is the sample size.

Results

Overall, we collected 277 POC_{susp} samples in the GOM. The $\delta^{13}C$ signatures (n = 277), and $\Delta^{14}C$ values (n = 123) are summarized in **Table 1**. POC_{susp} from the NCG euphotic zone (<300 m) had $\delta^{13}C$ signatures ranging from −17.8 to −35.4‰ (n = 108), with $\Delta^{14}C$ signatures from 54 to

Table 1: Summary statistics for blank-corrected $\delta^{13}C$ and $\Delta^{14}C$ signatures of POC_{susp} from all study sites during 2010–2017. DOI: https://doi.org/10.1525/elementa.389.t1

Location[a]	Depth[b]	δ¹³C Range (‰)	δ¹³C Mean ± S.D. (‰)	n	Δ¹⁴C Range (‰)	Δ¹⁴C Mean ± S.D. (‰)	n
Overall	Euphotic	−17.8 to −35.4	−24.3 ± 2.8	178	71 to −515	−96 ± 144	76
	Deep	−20.6 to −35.2	−27.1 ± 2.9	98	−48 to −756	−314 ± 197	48
NCG	Euphotic	−17.8 to −35.4	−24.1 ± 3.0	108	54 to −515	−98 ± 143	55
	Deep	−20.6 to −35.2	−27.1 ± 3.0	65	−48 to −603	−258 ± 162	39
Seep	Euphotic	−19.3 to −28.8	−24.4 ± 2.5	62	71 to −468	−128 ± 164	14
	Deep	−21.4 to −34.3	−27.1 ± 2.6	33	−263 to −756	−558 ± 139	9
WGOM	Euphotic	−22.8 to −29.2	−25.2 ± 2.1	8	51 to −204	−16 ± 85	7

[a] North central Gulf (NCG) samples were collected away from distinct areas of seepage; seep samples, over seep areas; western Gulf of Mexico (WGOM) samples, at the surface west of 94° longitude.
[b] Euphotic samples were collected above 300 m; deep samples, below 300 m.

−515‰ (n = 55). Deep-water particles (>300 m) from the NCG had δ^{13}C signatures ranging from −20.6 to −35.2‰ (n = 65), with Δ^{14}C signatures from −48 to −603‰ (n = 39). Seep euphotic POC_{susp} had δ^{13}C signatures ranging from −19.3 to −28.8‰ (n = 62), with Δ^{14}C signatures from 71 to −468‰ (n = 14). Deep-water suspended particles from seep sites had δ^{13}C signatures ranging from −21.4 to −34.3‰ (n = 33), with Δ^{14}C signatures from −263 to −756‰ (n = 9). POC_{susp} collected from the euphotic zone in the western GOM (WGOM, west of 94° longitude) had δ^{13}C signatures ranging from −22.8 to −29.2‰ (n = 8), with Δ^{14}C signatures from 51 to −204‰ (n = 7). All data are provided in Table S1.

The δ^{13}C and Δ^{14}C signatures for all POC_{susp} samples, across all collection depths and sampling years, were highly variable, as seen in **Figure 3** where the δ^{13}C and Δ^{14}C signatures of NCG POC_{susp} are color-coded by year. Suspended particles from seep sites were not color-coded by year, as the majority of the samples were collected in 2013. We observed two trends of δ^{13}C and Δ^{14}C

co-variation in the POC_{susp} data (**Figure 4**). One trend, the lower limb, indicated co-variation based on blending of modern surface production and petrocarbon input, observed for both NCG and seep sites. The upper limb, observed primarily for NCG sites, reflected the addition of another carbon source to modern production, with depleted δ^{13}C but more enriched Δ^{14}C signatures, possibly associated with the biodegradation of biogenic methane produced in the water column (Rakowski et al., 2015). In this study, we used two different mixing models to characterize both the co-variation based on petrocarbon input and the variation based on all of the sources that could contribute to GOM POC_{susp}.

Study-wide concentrations of POC_{susp} followed an expected gradient with highest concentrations at the surface decreasing with depth (**Figure 5**). Concentrations in the euphotic zone (<300 m) ranged from 0.32 to 62.5 μM (mean ± S.D.: 4.71 ± 9.38, n = 78). The four highest concentrations at the surface came from non-seep sites that were heavily influenced by
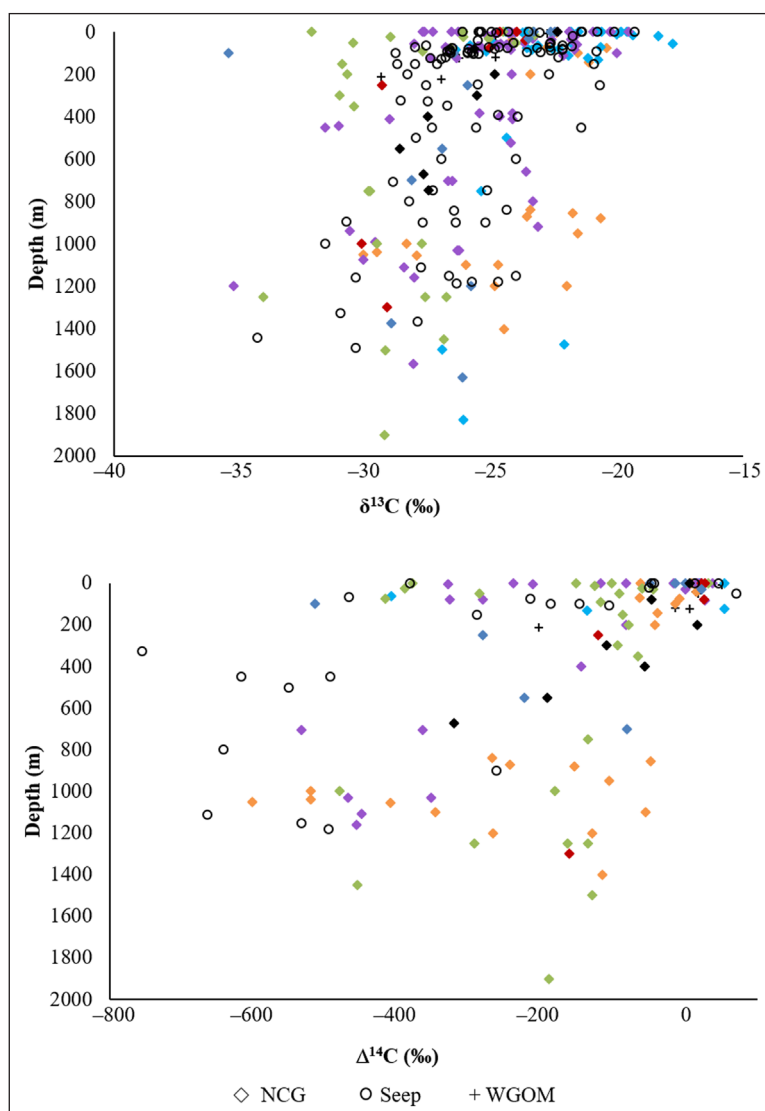

Figure 3: δ^{13}C and Δ^{14}C by depth for POC_{susp} collected in the GOM during 2010−2017. δ^{13}C (upper) and Δ^{14}C (lower) signatures of POC_{susp} by depth, color coded by collection year: orange for 2010; aqua, 2012; purple, 2013; green, 2014; red, 2015; blue, 2016; and black, 2017. Seep samples from all years are shown as open circles. Western Gulf of Mexico (WGOM) samples from 2016 (west of 94° longitude) are shown as plus symbols. DOI: https://doi.org/10.1525/elementa.389.f3
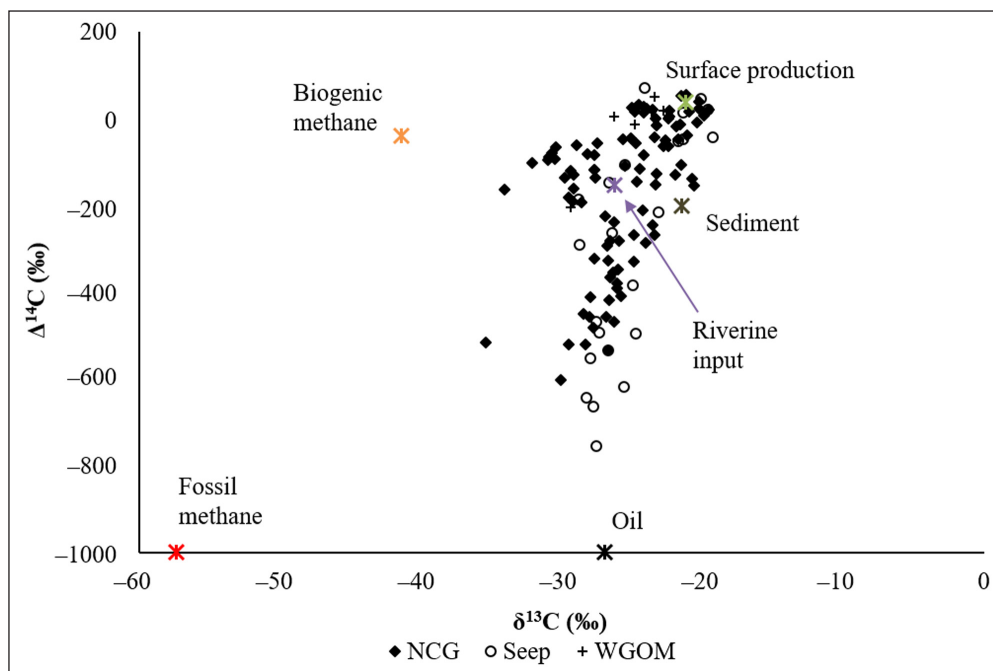
Figure 4: $\delta^{13}C$ vs $\Delta^{14}C$ of POC$_{susp}$ collected in the GOM during 2010−2017. Sites classified as: NCG (non-seep; diamonds), seep (open circles), and western GOM (WGOM, plus signs). Stars show main potential carbon sources to GOM POC$_{susp}$, including surface production (green), biogenic methane (orange), riverine input (purple), sediment (gray), fossil methane (red), and oil (black). DOI: https://doi.org/10.1525/elementa.389.f4
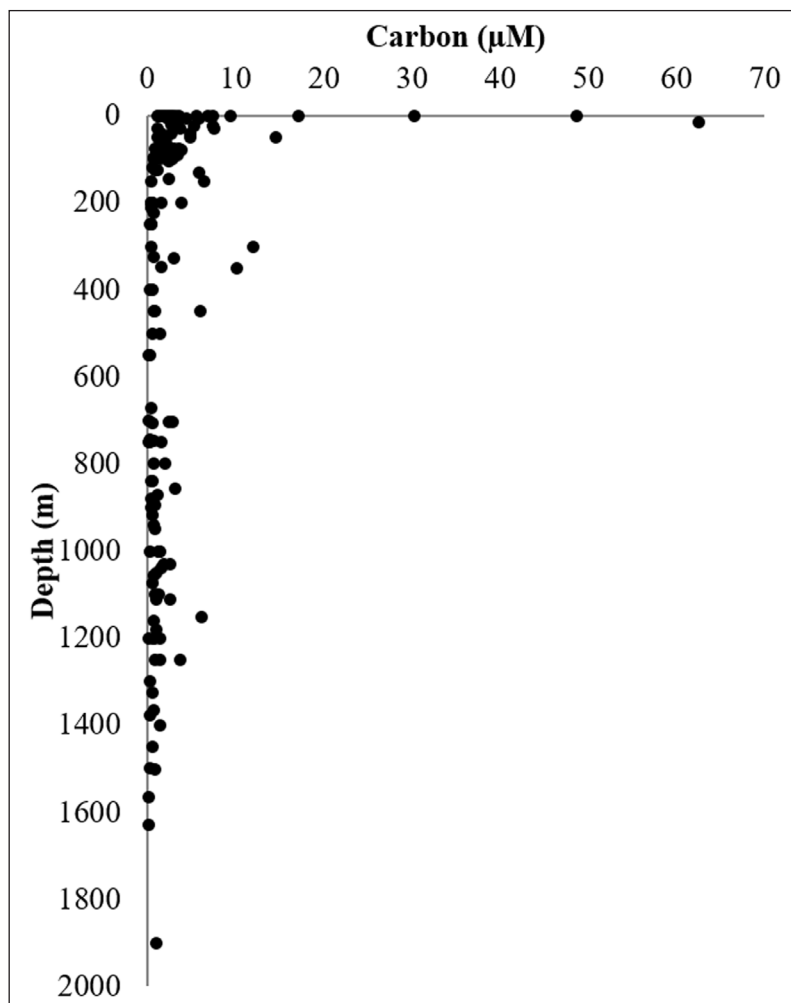

Figure 5: Carbon concentrations (µM) by depth for POC$_{susp}$ collected in the GOM during 2010−2017. Data are from all stations sampled in this study (Figure 2). DOI: https://doi.org/10.1525/elementa.389.f5

riverine input. Concentrations of POC_{susp} in deep water (>300 m) ranged from 0.16 to 12.02 μM C (mean ± S.D.: 1.44 ± 2, n = 72).

Temporal trends in carbon isotopes in POC_{susp}

We tested the hypothesis that $\delta^{13}C$ and $\Delta^{14}C$ of POC_{susp} in the north central Gulf at non-seep sites would vary temporally, becoming increasingly enriched in heavy isotopes following their depletion associated with the 2010 injection of fossil hydrocarbons into the water column from the DWH oil spill (Cherrier et al., 2014; Fernandez et al., 2016; Weber et al., 2016). We calculated the weighted averages of the non-seep NCG particles collected each year to create an inventory that accounts for the quantity of organic carbon contributing to the $\delta^{13}C$ and $\Delta^{14}C$ signatures (**Table 2**). Data from Cherrier et al. (2014) were included in 2011 and 2012. Data were separated by depth, into NCG euphotic and deep water (**Figure 6**). The $\delta^{13}C$ and $\Delta^{14}C$ of euphotic POC_{susp} and $\delta^{13}C$ of deep-water POC_{susp} (**Figure 6A–C**) exhibited depletion from 2010 to 2011. Afterwards the signatures increased in 2012, before decreasing again until 2014 and then increasing again and stabilizing by 2015. The $\Delta^{14}C$ of deep-water particles (**Figure 6D**) showed the clearest indication of fossil carbon incorporation, over a longer time period from 2010 to 2012 with recovery from 2012 to 2014, stabilizing in the following years (2015–2017) at around $\Delta^{14}C = -160‰$. During the recovery period of 2012–2014, the linear regression calculated between these two years suggested a recovery rate (in ‰ per year towards more ^{14}C enriched values) of 159‰ (**Figure 6D**).

Biogenic methane

Dissolved CH_4 concentrations in the water column varied from 2.6 to 11.6 nM, while the isotopic composition of methane varied from −37 to −52‰. A subsurface maximum in methane concentration was observed in both profiles within the euphotic zone at 60–75 m depth (**Figure 7**). The average $\delta^{13}C$ value, weighting the two profiles equally, was −41.4 ± 1.0‰ (n = 19). For the mixing model, we assumed that this methane was produced from modern

photosynthetic carbon, not derived from nearby seeps, and had a $\Delta^{14}C$ value of 39 ± 26‰ (n = 79). The $\delta^{13}C$ value we observed was similar to those measured in the Atlantic and Pacific oceans which varied between −43 and −45‰ (Holmes et al., 2000). Karl et al. (2008) have suggested that oceanic water column CH_4 is produced aerobically as a by-product of methylphosphonate decomposition in phosphate-stressed waters, supporting our assumption of a modern ^{14}C value for this methane. Rakowski et al. (2015) observed depletion of phosphate in the euphotic zone at the methane maximum, where we similarly observed it. The ^{13}C value is consistent with production from a methylated substrate in limited supply that is consumed quantitatively (Kelley et al., 2012; Tazaz et al., 2013).

Mixing models

The two-endmember mixing model indicated that the bulk of the carbon in POC_{susp} from the NCG euphotic (<300 m), seep euphotic and NCG deep (>300 m) sites was derived from modern surface production (**Table 3**). In contrast to seep euphotic, seep deep POC_{susp} had incorporated the most petrocarbon, averaging 57% ± 13 (n = 9), while NCG deep POC_{susp} averaged 29% ± 16 (n = 39) petrocarbon (**Table 3**). Our sensitivity test showed the greatest variation in the euphotic POC_{susp}, where $\Delta^{14}C$ was close to the modern endmember. The two-endmember model estimations of the %modern for the euphotic test samples were within 2–3% of the model values, and the %petrocarbon estimations also varied by 2–3%. The deep-water source estimations varied by 0–1% for both %modern and %petrocarbon.

The MixSIAR model (**Table 3**) suggested that POC_{susp} in the north central GOM is heavily derived from riverine inputs (up to 46%), followed by modern surface production (up to 45%), and, at seep deep sites, by oil (up to 46%). All deep-water POC_{susp} had higher contributions from hydrocarbons than euphotic POC_{susp}. Euphotic POC_{susp} at seep sites also had higher contributions from oil-derived carbon than at NCG euphotic sites; i.e., 8.2 ± 3.6% (n = 14) compared to 2.0 ± 1.2% (n = 55). Sediment, fossil methane, and biogenic methane contributed very little to the organic carbon in POC_{susp}, with high standard deviations of their means.

Table 2: Weighted averages for $\delta^{13}C$ and $\Delta^{14}C$ signatures of POC_{susp} from NCG sites during 2010–2017. DOI: https://doi.org/10.1525/elementa.389.t2

Year	Euphotic POC_{susp}			Deep POC_{susp}		
	POC_{susp} (μM)	Wt.Avg $\Delta^{14}C$ (‰)	Wt.Avg $\delta^{13}C$ (‰)	POC_{susp} (μM)	Wt.Avg $\Delta^{14}C$ (‰)	Wt.Avg $\delta^{13}C$ (‰)
2010	26.2	−18	−22.2	20.7	−291	−25.9
2011	61.4	−64	−27.4	18.8	−415	−34.4
2012	234.5	−11	−20.7	50.4	−528	−26.2
2013	122.4	−120	−24.8	42.8	−427	−26.6
2014	188.1	−149	−27.6	35.2	−152	−31.0
2015	14.5	20	−24.5	0.5	−161	−28.7
2016	11.1	−52	−23.7	1.1	−147	−26.7
2017	4.2	−19	−24.2	1.8	−185	−27.1
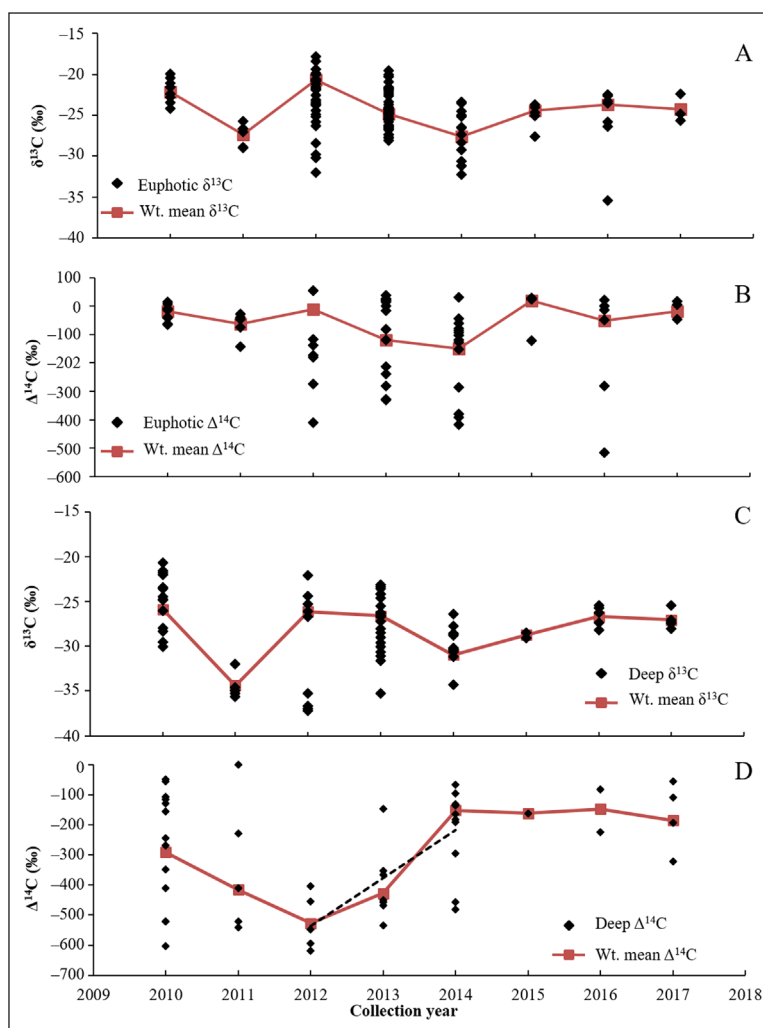
Figure 6: Temporal trends in δ¹³C and Δ¹⁴C of POC$_{susp}$ collected from NCG sites during 2010−2017. A) δ¹³C and **B)** Δ¹⁴C of POC$_{susp}$ from NCG (non-seep) euphotic (<300 m), and **C)** δ¹³C and **D)** Δ¹⁴C of POC$_{susp}$ from NCG deep (>300 m). Red squares indicate the weighted mean for each sampling year; red lines are visual guides of possible trends. Black dashed line from 2012 to 2014 in D) indicates linear regression (y = 159.58x − 321604, n = 43, r = 0.7258, p < 0.0001) as a measure of recovery rate. Each panel includes data from Cherrier et al. (2014) for 2011 and 2012. DOI: https://doi.org/10.1525/elementa.389.f6
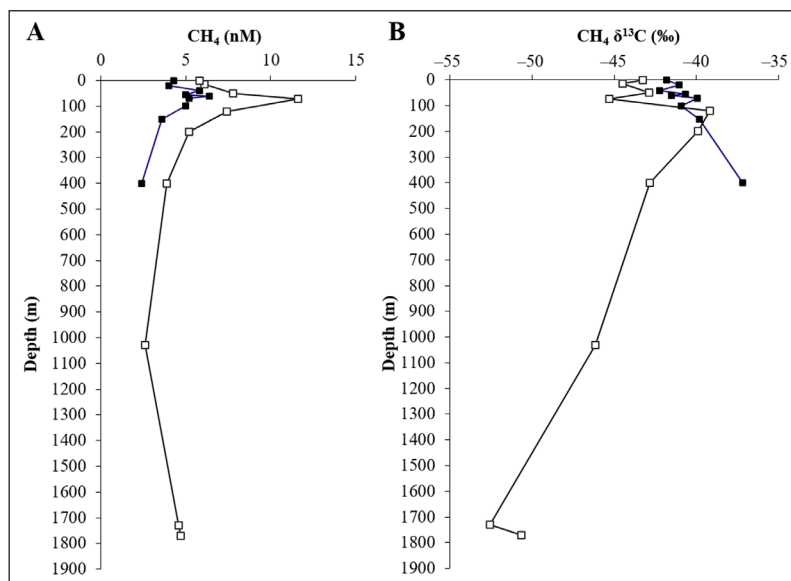

Figure 7: Depth profiles of biogenic methane concentration and δ¹³C signature. A) Methane concentration and **B)** δ¹³C for methane at two sites: 28.6690 N, 88.3584 W, closed symbols; and 28.3255 N, 88.3865 W, open symbols (see Figure 2). DOI: https://doi.org/10.1525/elementa.389.f7

Table 3: Percent (%) contributions of carbon sources to POC$_{susp}$ from a two-endmember mixing model and the MixSIAR model. DOI: https://doi.org/10.1525/elementa.389.t3

Site type	Sample depth[a]	Two-endmember mixing model					MixSIAR mixing model						
		Modern surface production		Petrocarbon		n	Modern surface production	Riverine input	Sediment	Oil	Fossil methane	Biogenic methane	n
		Mean ± SD	Range	Mean ± SD	Range		Mean ± SD	Mean ± SD	Mean ± SD	Mean ± SD	Mean ± SD	Mean ± SD	
NCG[b]	Euphotic	86 ± 14	47–100	14 ± 14	0–53	53	45.1 ± 11.0	41.2 ± 12.5	4.3 ± 5.6	2.0 ± 1.2	2.2 ± 1.9	5.2 ± 3.5	55
	Deep	71 ± 16	38–92	29 ± 16	8–62	39	19.9 ± 10.0	46.3 ± 11.8	6.0 ± 6.0	15.4 ± 4.1	4.3 ± 2.9	8.1 ± 4.8	39
Seep	Euphotic	81 ± 15	51–98	19 ± 15	2–49	12	39.0 ± 12.4	44.5 ± 13.7	3.8 ± 5.9	8.2 ± 3.6	1.5 ± 1.4	3.0 ± 2.5	14
	Deep	43 ± 13	23–71	57 ± 13	29–76	9	11.6 ± 6.1	33.7 ± 8.2	3.4 ± 3.8	45.7 ± 5.3	2.3 ± 1.8	3.4 ± 2.6	9

[a] Euphotic indicates <300 m; deep, >300 m.
[b] Non-seep north central Gulf (NCG) sites.

Broader context

To characterize POC$_{susp}$ in the broader context of the GOM, we plotted the $\delta^{13}C$ and $\Delta^{14}C$ signatures for other carbon reservoirs in the GOM, including: POC$_{sink}$, non-seep sediment, seep sediment, and DIC (**Figure 8**). We also included signatures (as provided in Methods) for the different potential carbon sources to these pools, including modern surface production, riverine input, sediment, biogenic methane, DWH methane, and oil (**Figure 8**).

Statistics

The data were non-normally distributed; therefore, the non-parametric Mann-Whitney U tests were used to analyze the variation of $\delta^{13}C$ and $\Delta^{14}C$ signatures of POC$_{susp}$, from 2010 to 2017. We compared the importance of depth in the water column (euphotic <300 m or deep >300 m) and site type (NCG or seep) in determining the isotopic signatures of POC$_{susp}$ (**Tables 4** and **5**) using the adjusted p-value of 0.008 to define significance. There were significant differences in $\delta^{13}C$ signatures when comparing between depths, regardless of site classification.

For instance, the median values for $\delta^{13}C$ of POC$_{susp}$ from NCG euphotic (−24.1‰) and NCG deep (−27.0‰) were significantly different (U = 1656, p < 0.001, r = 0.43), as were those for NCG deep (−27.0‰) and seep euphotic (−24.8‰) (U = 992, p < 0.001, r = 0.42). Comparisons $\delta^{13}C$ of POC$_{susp}$ involving the same depth zones yielded similarities: the median value for NCG euphotic (−24.1‰) did not differ from that for seep euphotic (−24.8‰) (U = 3065, p = 0.27, r = 0.08), nor did the median for NCG deep (−27.0‰) differ from that of seep deep (−27.0‰) (U = 1034, p = 0.96, r = 0.003). For radiocarbon, comparisons between different depth zones revealed significantly different $\Delta^{14}C$ signatures, except when comparing median values for NCG deep (−224‰) and seep euphotic (−78‰), which were similar (U= 132, p = 0.007, r = −0.37). POC$_{susp}$ from the NCG euphotic and euphotic seep (medians of −60‰ and −78‰, respectively) were the same (U = 359, p = 0.56, r = 0.07), but unlike $\delta^{13}C$, there were significant differences between NCG deep (median = −224‰) and seep deep (median = −552‰) (U = 28, p < 0.001, r = 0.56) (**Table 5**).
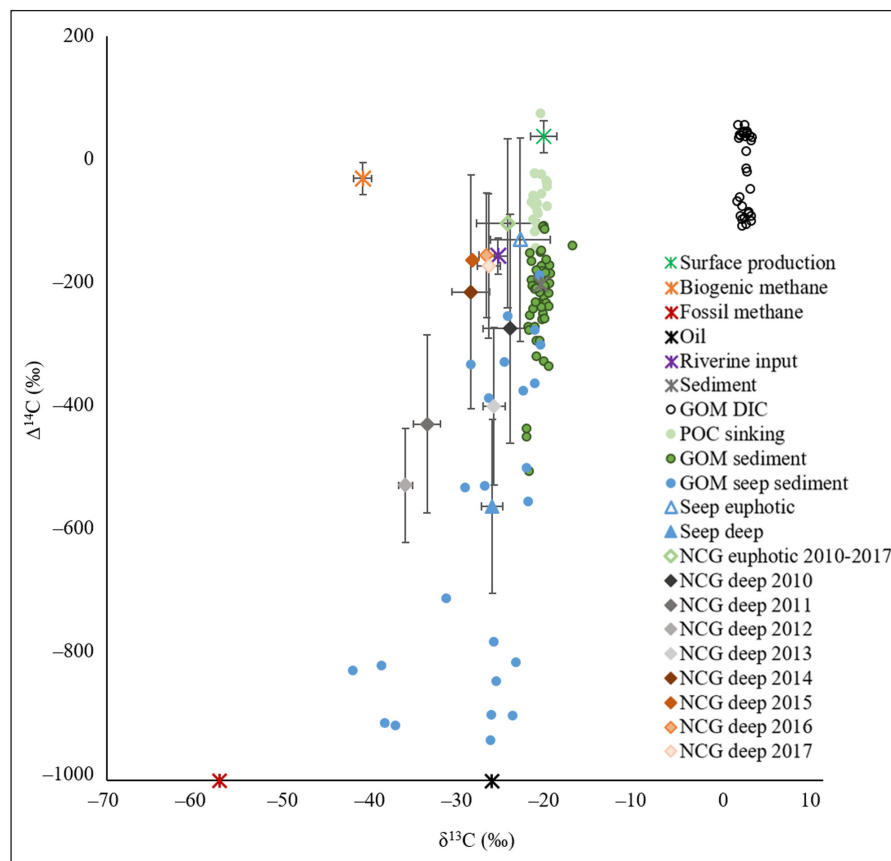

Figure 8: Carbon source endmembers and other carbon pools in the GOM. Plot of $\delta^{13}C$ vs $\Delta^{14}C$ of carbon endmembers and of POC$_{susp}$ (this study and Cherrier et al., 2014, for NCG Deep 2011 and 2012), POC$_{sink}$ (Yan et al., 2016), GOM sediment (Chanton et al., 2015), GOM seep sediment (Chanton, 2018a), and GOM DIC (Chanton, 2018b). Data for POC$_{susp}$ are presented by depth, with NCG euphotic (<300 m) from 2010–2017 grouped together (green open diamond) and NCG deep (>300 m) separated by year and listed at the bottom of the inset legend. Seep site POC$_{susp}$ is indicated by blue triangles. Endmembers include surface production (green, $\delta^{13}C$ = −21.2 ± 1.5‰, n = 82; $\Delta^{14}C$ = 39 ± 26‰, n = 79), fossil methane (red, $\delta^{13}C$ = −57.4 ± 0.4‰, Crespo-Medina et al., 2014; $\Delta^{14}C$ = −1000‰), and oil (black, $\delta^{13}C$ = −27‰; $\Delta^{14}C$ = −1000‰), riverine input (purple, $\delta^{13}C$ = −26.3 ± 1.1‰; $\Delta^{14}C$ = −154 ± 68‰, Cai et al., 2015), sediment (grey, $\delta^{13}C$ = −21.5 ± 0.8‰; $\Delta^{14}C$ = −200 ± 29‰, Chanton et al., 2015) and biogenic methane (orange, $\delta^{13}C$ = −41.4 ± 1.0‰, n = 19; $\Delta^{14}C$ = −39 ± 26‰, n = 79). DOI: https://doi.org/10.1525/elementa.389.f8

Table 4: Mann-Whitney U Test for $\delta^{13}C$ comparisons for samples collected during 2010–2017. DOI: https://doi.org/10.1525/elementa.389.t4

Treatment pair	Median	Range	n	U	P	r
NCG euphotic vs NCG deep	−24.1	−17.8 to −35.4	110	1656	p < 0.001	0.43
	−27.0	−20.6 to −35.2	63			
NCG euphotic vs seep euphotic	−24.1	−17.8 to −35.4	110	3065	p = 0.27	0.08
	−24.8	−19.3 to −28.8	62			
NCG euphotic vs seep deep	−24.1	−17.8 to −35.4	110	755	p < 0.001	0.42
	−27.0	−21.4 to −34.3	33			
NCG deep vs seep euphotic	−27.2	−20.6 to −35.2	63	992	p < 0.001	0.42
	−24.8	−19.3 to −28.8	62			
NCG deep vs seep deep	−27.2	−20.6 to −35.2	63	1034	p = 0.96	0.003
	−27.0	−21.4 to −34.3	33			
Seep euphotic vs seep deep	−24.8	−19.3 to −28.8	62	8486	p < 0.001	0.43
	−27.0	−21.4 to −34.3	33			

Table 5: Mann-Whitney U Test for $\Delta^{14}C$ comparisons for samples collected during 2010–2017. DOI: https://doi.org/10.1525/elementa.389.t5

Treatment pair	Median	Range	n	U	P	r
NCG euphotic vs NCG deep	−60	54 to −515	57	394	p < 0.001	0.53
	−224	−48 to −603	37			
NCG euphotic vs seep euphotic	−60	54 to −515	57	359	p = 0.56	0.07
	−78	71 to −468	14			
NCG euphotic vs seep deep	−60	54 to −515	57	12	p < 0.001	0.57
	−552	−263 to −756	9			
NCG deep vs seep euphotic	−224	−48 to −603	37	132	p = 0.007	−0.37
	−78	71 to −468	14			
NCG deep vs seep deep	−224	−48 to −603	37	28	p < 0.001	0.56
	−552	−263 to −756	9			
Seep euphotic vs seep deep	−78	71 to −468	14	3	p < 0.001	0.77
	−552	−263 to −756	9			

Discussion

The first goal of this study was to characterize any temporal trends in the $\delta^{13}C$ and $\Delta^{14}C$ signatures of suspended POC in the northern Gulf of Mexico following the DWH oil spill in 2010. Isotopically depleted values for POC_{susp} indicating a fossil petrocarbon source were observed following the spill (**Figure 6**), particularly in the ^{14}C content of suspended particles below the euphotic zone at NCG sites. The influence of apparent DWH-derived material was greatest in 2011 and 2012, with recovery beginning thereafter and proceeding until 2014 when the isotopic composition of POC_{susp} reached an asymptotic value (**Figure 6**).

Yan et al. (2016), Chanton et al. (2018), and Geiring et al. (2018) described the effects and recovery of the POC_{sink} pool following the blowout. Yan et al. (2016) found elevated levels of barium, a component of drilling mud, in POC_{sink} from August 2010 through January 2011, when they returned to pre-spill baseline levels. Chanton et al. (2018) found that POC_{sink} recovered in 1–3 years depending on the tracer that was evaluated. $\delta^{34}S$ and PAH indicated an approximate 2-year recovery time, while $\Delta^{14}C$ indicated a recovery time of ~3 years. These recovery periods are on a similar time scale to our estimate of a 4-year recovery period in the $\Delta^{14}C$ of POC_{susp} in deep water at NCG sites (**Figure 6**).

A second goal was to determine the extent of fossil carbon influence on suspended particles. We found a wide range of natural variability in both $\delta^{13}C$ and $\Delta^{14}C$ signatures of POC_{susp} across the northern GOM, from seep and non-seep sites and a range of depths, from surface to 1900 m (**Figure 3**). Compared to suspended particles in the Sargasso Sea and Pacific Station M, the GOM exhibits more variability and greater depletion in $\delta^{13}C$ and $\Delta^{14}C$

signatures (**Figure 1**; Druffel et al., 1992, 1996). The primary carbon source to the Sargasso and Pacific particulates is modern photosynthetic production, which does not create a co-variation of $\delta^{13}C$ with $\Delta^{14}C$. The depletion in $\Delta^{14}C$ in the Sargasso and mid-Pacific was not observed to be greater than −100‰, even to depths of 4000 m. The $\delta^{13}C$ value of the Pacific and Atlantic suspended particles was generally −20 to −22‰ without depth variation. The co-variation of $\delta^{13}C$ and $\Delta^{14}C$ observed in the GOM and the Mid-Atlantic Bight (as presented in the Introduction) are due to the incorporation of a second source that is depleted in both ^{14}C and ^{13}C, consistent with petrocarbon-derived material. In the Southern Gulf of Mexico from 20° to 22°N, Gonzalez-Ocampo et al. (2007) reported POC_{susp} depth trends in $\delta^{13}C$, with ^{13}C depletion at depth reaching values as low as −23.7 ± 0.5‰. Values in surface water were −22.5 ± 0.5‰.

We admit some reservations about the results of the MixSIAR mixing model, as two of our sources, riverine input and sedimentary organic carbon had some surprising results. The MixSIAR model was used to constrain six carbon sources with two isotopic tracers. The riverine input (34–46%) was estimated to be greater than the input from surface production (11.6–45.1%) for all sites except NCG euphotic (riverine: 41%; surface production: 45%). For the workings of the model, the riverine endmember was located isotopically in the middle of the bulk of the POC_{susp} values, rather than along the boundary of our data (**Figure 4**). This location could cause the model to estimate a higher percent contribution to POC_{susp} because of the isotopic similarities between the POC_{susp} and riverine input. The data might well represent mixing between modern carbon and a more depleted source. On the other hand, the apparent high riverine contribution may be due to the differences in lability between the riverine and modern sources. Riverine carbon is less labile than fresher photosynthetic production, which causes it to cycle more slowly than surface production (Wang et al., 2004). The salinity at the stations where we collected POC_{susp} varied (Table S1), but most sites did not indicate major mixing with freshwater sources. However, Wang et al. (2004) found that $\delta^{13}C$ and C:N ratios of POC_{susp} from the Mississippi and northern GOM exhibited non-conservative behavior when mixing with higher salinity waters. A decoupling occurs between the POC_{susp} and the freshwater input which allows the 2.30 Tg POC yr^{-1} exported from the Mississippi (Cai et al., 2015) to mix with GOM POC_{susp} and accumulate over the POC_{susp} residence time of 5–10 years, increasing the contribution from riverine POC_{susp}.

Whereas the riverine contribution to POC_{susp} was higher than expected, the sedimentary contribution was low and consistent throughout the water column. Chanton et al. (2018) found that sinking POC, collected from traps 30 m above the seafloor, did not carry a strong signal from resuspended sediment, but POC_{susp} integrates over longer time scales. Diercks et al. (2018) detected both small-scale and hurricane-sized resuspension events, which could play a role in the transport of sedimented petrocarbon. The number and overall scale of resuspension events in the GOM is unknown, but they potentially introduce more than 4–6% into the POC_{susp} pool, especially near the seafloor. The sedimentary organic carbon endmember is similar in isotope space to riverine input (**Figure 4**), making the two sources difficult to separate. Employing sulfur isotopes and lithogenic silica content might better separate sedimentary and riverine sources.

Unlike the MixSIAR model, the two-endmember model is simpler and better constrained. This model indicated the local influence of seeps, particularly on deep-water POC_{susp}, and the importance of modern surface production on POC_{susp} away from seeps (**Table 3**). Nonetheless, petrocarbon still contributed about 30% of POC_{susp} in the deep GOM, even away from seep sites, a phenomenon not observed in the Atlantic or Pacific. Even though the two-endmember model does not capture the full complexity of all of the potential sources to POC_{susp} in the GOM, the results of the MixSIAR model, using only two isotopic measurements, can only be fully interpreted with reservations, for the aforementioned reasons. Therefore, we have greater confidence in the two-endmember approach.

We estimated the new, post-spill baseline signatures for NCG (non-seep) POC_{susp} in the GOM to be $\delta^{13}C = -24.1 ± 0.4‰$ (n = 15) and $\Delta^{14}C = -17 ± 36‰$ (n = 15) for the euphotic zone and $\delta^{13}C = -27.5 ± 1.1‰$ (n = 12) and $\Delta^{14}C = -164 ± 19‰$ (n = 7) for deep-water suspended particles. These values are the means of the POC_{susp} weighted averages from the NCG for the last three sampling years (2015–2017; **Figure 6**). Following the recovery of deep-water $\Delta^{14}C$ signatures in 2014, we suggest that POC_{susp} reached a post-blowout baseline, as both the $\delta^{13}C$ and $\Delta^{14}C$ signatures had stabilized by these years. In comparison to baselines from the Sargasso Sea and Pacific Ocean, the baseline for POC_{susp} from the GOM was more depleted for $\delta^{13}C$ and $\Delta^{14}C$. We estimated the $\delta^{13}C$ and $\Delta^{14}C$ baselines for POC_{susp} collected in the Sargasso and Pacific (Druffel et al., 1992, 1996, 2003) for our depth zones to be: euphotic $\delta^{13}C = -22.1‰$ (n = 41) and $\Delta^{14}C = 73$ (n = 42); and deep POC_{susp} $\delta^{13}C = -21.2‰$ (n = 82) and $\Delta^{14}C = 16‰$ (n = 83). The differences in $\delta^{13}C$ between the GOM and the Sargasso and Pacific are due to differences in the increased relative importance of hydrocarbon and terrestrially sourced material to the GOM, while the $\Delta^{14}C$ differences are caused by both collection years and the relative importance of differing carbon sources. The gap of 22–32 years between the collection of the Sargasso and Pacific samples and our samples results in the older samples being more enriched in ^{14}C. This effect is due to the atmospheric nuclear testing that caused radiocarbon values to spike and mix from the atmosphere into the biosphere and hydrosphere, including the ocean. The mixing process caused a lag between atmospheric CO_2 radiocarbon signatures and DIC in the ocean (Levin and Hesshaimer, 2000; McNichol and Aluwihare, 2007).

Unlike POC_{susp} from the Sargasso Sea and Pacific Ocean, depth played a significant role in the variation of $\delta^{13}C$ of POC_{susp} in the GOM over the period of 2010–2017. The significant differences observed between euphotic (<300 m) and deep (>300 m) reflect the relative importance of the two sources, with petrocarbon-derived material increasing in importance below 300 m (**Tables 2** and **4**). Suspended particles in deep water were depleted

due to the hydrocarbon input potentially from seep sites and/or the DWH blowout, while POC$_{susp}$ from the same depth (whether euphotic or deep) had similar δ^{13}C, regardless of site type (seep or NCG).

We also found significant differences between the Δ^{14}C of POC$_{susp}$ in euphotic and deep POC$_{susp}$ for both site types (seep or NCG) (**Table 5**). This finding suggests that suspended particles in the GOM, including at non-seep sites, are more depleted in ^{14}C in deeper waters than suspended particles in other oceans, probably due to the natural hydrocarbon seepage in the GOM, although completely ruling out the lingering petrocarbon from the oil spill is difficult at this point. The significant differences between the Δ^{14}C of deep-water POC$_{susp}$ from NCG and seep areas were not observed for the δ^{13}C results, as δ^{13}C is less sensitive to variations in the input terms (Bosman et al., 2016). The more depleted Δ^{14}C of POC$_{susp}$ found at seep sites suggests that the presence of natural hydrocarbon seepage significantly affects the Δ^{14}C of suspended particles in the Gulf.

Conclusions

Based on our assessment of the δ^{13}C and Δ^{14}C signatures of POC$_{susp}$, petrocarbon is an important carbon source to suspended particles in the GOM, in contrast to the situation in the Atlantic and Pacific oceans. In the north central Gulf during our study period, POC$_{susp}$ was isotopically depleted relative to POC$_{sink}$ or sediment (**Figure 8**). DIC fixed by marine primary production is the primary source of carbon to POC$_{sink}$ and to the non-seep sediment. We found deep POC$_{susp}$ from seep sites to be composed of about 45% oil-derived petrocarbon, while deep-water POC$_{susp}$ from the NCG sites may contain as much as 15% oil-sourced petrocarbon and 3.5% methane-sourced petrocarbon. In the Gulf of Mexico, there are at least three clear and separate carbon sources (**Figure 8**): one driven by surface primary production, observed in POC$_{sink}$ and non-seep sediments; the second attributed to the microbial cycling of methane and oil, observed to a greater extent in POC$_{susp}$ and seep sediments; and the third, a riverine contribution, pervasive but more challenging to quantify unambiguously.

Data Accessibility Statement

Data deposition: Data are publicly available through the Gulf of Mexico Research Initiative Information & Data Cooperative (GRIIDC) at https://data.gulfresearchinitiative.org, 10.7266/N7FX77C7.

Supplemental file

The supplemental file for this article can be found as follows:

· **Table S1.** POC$_{susp}$ sample collection and isotope data. DOI: https://doi.org/10.1525/elementa.389.s1

Competing interests

The authors have no competing interests to declare.

Author contributions

· KLR wrote the paper with JPC, collected samples, analyzed samples and data
· SB edited the paper, collected samples, analyzed samples and data
· SW collected samples, analyzed samples
· CM collected samples, analyzed samples
· JPM collected samples analyzed data
· JPC co-wrote the paper, analyzed data

References

Bacon, MP and **Anderson, RF.** 1982. Distribution of Thorium isotopes between dissolved and particulate forms in the deep sea. *J Geophys Res* **87**(C3): 2045–2056. DOI: https://doi.org/10.1029/JC087iC03p02045

Bauer, JE and **Druffel, ERM.** 1998. Ocean margins as a significant source of organic matter to the deep open ocean. *Nature* **392**: 482–485. DOI: https://doi.org/10.1038/33122

Bauer, JE, Druffel, ERM, Wolgast, DM and **Griffin, S.** 2001. Sources and cycling of dissolved and particulate organic radiocarbon in the northwest Atlantic continental margin. *Global Biogeochem Cy* **15**(3): 615–636. DOI: https://doi.org/10.1029/2000GB001314

Bauer, JE, Druffel, ERM, Wolgast, DM and **Griffin, S.** 2002. Temporal and regional variability in sources and cycling of DOC and POC in the northwest Atlantic continental shelf and slope. *Deep Sea Res Pt II* **49**: 4387–4419. DOI: https://doi.org/10.1016/S0967-0645(02)00123-6

Börjesson, G, Chanton, J and **Svensson, BH.** 2001. Methane oxidation in two Swedish landfill

covers measured with carbon-13 to carbon-12 isotope ratios. *J Environ Qual* **30**(2): 369–376. DOI: https://doi.org/10.2134/jeq2001.302369x

Börjesson, G, Sundh, I, Tunlid, A, Frostegård, Å and **Svensson, BH.** 1998. Microbial oxidation of CH_4 at high partial pressures in an organic landfill cover soil under different moisture regimes. *FEMS Microbiol Ecol* **26**(3): 207–217. DOI: https://doi.org/10.1111/j.1574-6941.1998.tb00506.x

Cai, Y, Guo, L, Wang, X and **Aiken, G.** 2015. Abundance, stable isotopic composition, and export fluxes of DOC, POC, and DIC from the Lower Mississippi River during 2006–2008. *J Geophys Res Biogeosci* **120**: 2273–2288. DOI: https://doi.org/10.1002/2015JG003139

Carlson, CA and **Hansell, DA.** 2014. DOM sources, sinks, reactivity, and budgets. In Hansell, DA and Carlson, CA (eds.), *Biogeochemistry of marine dissolved organic matter (second edition)*. Maine: Elsevier Inc. DOI: https://doi.org/10.1016/B978-0-12-405940-5.00003-0

Chanton, J. 2018a. Sediment organic isotope data collected in the northern Gulf of Mexico seafloor on different cruises from 2010-05-01 to 2017-06-18. Distributed by: Gulf of Mexico Research Initiative Information and Data Cooperative (GRIIDC), Harte Research Institute, Texas A&M University-Corpus Christi. DOI: https://doi.org/10.7266/N7Q52N7D

Chanton, J. 2018b. Dissolved Inorganic Carbon ^{14}C values, northern Gulf of Mexico, May 2011 to May 2012. Distributed by: Gulf of Mexico Research Initiative Information and Data Cooperative (GRIIDC), Harte Research Institute, Texas A&M University-Corpus Christi. https://data.gulfresearchinitiative.org/pelagos-symfony/data/R4.x268.000%3A0104. DOI: https://doi.org/10.7266/N7W37TWR

Chanton, J and **Lewis, FG.** 2002. Examination of coupling between primary and secondary production in a river-dominated estuary: Apalachicola Bay, Florida, U.S.A. *Limnol Oceanogr* **47**(3): 683–697. DOI: https://doi.org/10.4319/lo.2002.47.3.0683

Chanton, J, Zhao, T, Rosenheim, BE, Joye, S, Bosman, S, Brunner, C, Yeager, KM, Diercks, AR and **Hollander, D.** 2015. Using natural abundance radiocarbon to trace the flux of petrocarbon to the seafloor following the deepwater horizon oil spill. *Environ. Sci. Technol* **49**: 847–854. DOI: https://doi.org/10.1021/es5046524

Chanton, JP, Cherrier, J, Wilson, RM, Sarkodee-Adoo, J, Bosman, S, Mickle, A and **Graham, WM.** 2012. Radiocarbon evidence that carbon from the Deepwater Horizon spill entered the planktonic food web of the Gulf of Mexico. *Environ Res Lett* **7**(4). DOI: https://doi.org/10.1088/1748-9326/7/4/045303

Chanton, JP, Giering, SLC, Bosman, SH, Rogers, KL, Sweet, J, Asper, VL, Diercks, AR and **Passow, U.** 2018. Isotopic composition of sinking particles: Oil effects, recovery and baselines in the Gulf of Mexico,

2010–2015. *Elem Sci Anth* **6**: 43. DOI: https://doi.org/10.1525/elementa.298

Cherrier, J, Sarkodee-Adoo, J, Guilderson, TP and **Chanton, JP.** 2014. Fossil carbon in particulate organic matter in the Gulf of Mexico following the Deep Water Horizon event. *Environ Sci Technol Lett* **1**: 108–112. DOI: https://doi.org/10.1021/ez400149c

Crespo-Medina, M, Meile, CD, Hunter, KS, Diercks, A-R, Asper, VL, Orphan, VJ, Tavormina, PL, Nigro, LM, Battles, JJ, Chanton, JP, Shiller, AM, Joung, D-J, Amon, RMW, Bracco, A, Montoya, JP, Villareal, TA, Wood, AM and **Joye, SB.** 2014. The rise and fall of methanotrophy following a deepwater oil-well blowout. *Nat Geosci* **7**: 423–427. DOI: https://doi.org/10.1038/ngeo2156

Deuser, WG. 1986. Seasonal and interannual variations in deep-water particle fluxes in the Sargasso Sea and their relation to surface hydrography. *Deep Sea Res* **33**: 225–246. DOI: https://doi.org/10.1016/0198-0149(86)90120-2

Diercks, AR, Dike, C, Asper, VL, DiMarco, SF, Chanton, JP and **Passow, U.** 2018. Scales of seafloor sediment resuspension in the northern Gulf of Mexico. *Elem Sci Anth* **6**(32): DOI: https://doi.org/10.1525/elementa.285

Druffel, ERM, Bauer, JE, Griffin, S and **Hwang, J.** 2003. Penetration of anthropogenic carbon into organic particles of the deep ocean. *Geophys Res Lett* **30**(14). DOI: https://doi.org/10.1029/2003GL017423

Druffel, ERM, Bauer, JE, Williams, PM, Griffin, S and **Wolgast, D.** 1996. Seasonal variability of particulate organic radiocarbon in the northeast Pacific Ocean. *J Geophys Res* **101**(C9): 20543–20552. DOI: https://doi.org/10.1029/96JC01850

Druffel, ERM, Williams, PM, Bauer, JE and **Ertel, JR.** 1992. Cycling of dissolved and particulate organic matter in the open ocean. *J Geophys Res* **97**(C10): 15639–15659. DOI: https://doi.org/10.1029/92JC01511

Du, M and **Kessler, JD.** 2012. Assessment of the spatial and temporal variability of bulk hydrocarbon respiration following the Deepwater Horizon oil spill. *Environ Sci Technol* **46**(19): 10499–10507. DOI: https://doi.org/10.1021/es301363k

Fernández-Carrera, A, Rogers, KL, Weber, SC, Chanton, JP and **Montoya, JP.** 2016. Deep Water Horizon oil and methane carbon entered the food web in the Gulf of Mexico. *Limnol Oceanogr* **61**: S387–S400. DOI: https://doi.org/10.1002/lno.10440

Gonzalez-Ocampo, M, Escobar-Briones, E and **Morales-Puente, P.** 2007. Composición y caracterización isotopica δ^{13}C de carbono organico particulado en aguas oceanicas del suroeste de Golfo de Mexico. In: Hernandezdela Torre, B and Castro, GG (eds.). *Carbon en ecosistemas acuaticos de Mexico. Secretaria de Medio Ambiente y Recursos Naturales, Instituto Nacional de Ecologiea, Centro de*

Investigación Científica, y de Educación Superior de Ensenada. Ensenada, BC, Mexico.

Graham, WM, Condon, RH, Carmichael, RH, D'Ambra, I, Patterson, HK, Linn, LJ and **Hernandez, FJ, Jr.** 2010. Oil carbon entered the coastal planktonic food web during the Deepwater Horizon oil spill. *Environ Res Lett* **5**(4): 045301. DOI: https://doi.org/10.1088/1748-9326/5/4/045301

Holmes, ME, Sansone, FJ, Rust, TM and **Popp, BN.** 2000. Methane production, consumption and air-sea exchange in the open ocean: An evaluation based on carbon isotopic ratios. *Global Biogeochem Cy* **14**(1): 1–10. DOI: https://doi.org/10.1029/1999GB001209

Joye, SB, MacDonald, IR, Leifer, I and **Asper, V.** 2011. Magnitude and oxidation potential of hydrocarbon gases released from the BP oil well blowout. *Nat Geosci* **4**(3): 160–164. DOI: https://doi.org/10.1038/ngeo1067

Karl, DM, Beversdorf, L, Björkman, KM, Church, MJ, Martinez, A and **Delong, EF.** 2008. Aerobic production of methane in the sea. *Nat Geosci* **1**: 473–478. DOI: https://doi.org/10.1038/ngeo234

Kelley, CA, Poole, JA, Tazaz, AM, Chanton, JP and **Bebout, BM.** 2012. Substrate limitation for methanogenesis in hypersaline environments. *Astrobiology* **12**(2): 89–97. DOI: https://doi.org/10.1089/ast.2011.0703

Kessler, JD. 2011. A persistent oxygen anomaly reveals the fate of spilled methane in the deep Gulf of Mexico. *Science* **331**: 312–315. DOI: https://doi.org/10.1126/science.1199697

Lehr, W, Bristol, S and **Possolo, A.** 2010. Federal interagency solutions group, oil budget calculator science and engineering team. *Oil Budget Calculator.* Technical document. Available at http://www.restorethegulf.gov/sites/default/files/documents/pdf/OilBudgetCalc_Full_HQ-Print_111110.pdf.

Levin, I and **Hesshaimer, V.** 2000. Radiocarbon – a unique tracer of global carbon cycle dynamics. *Radiocarbon* **42**(1): 69–80. DOI: https://doi.org/10.1017/S0033822200053066

MacDonald, IR, Garcia-Pineda, O, Beet, A, Daneshgar Asl, S, Feng, L, Graettinger, G, French-McCay, D, Holmes, J, Hu, C, Huffer, F, Leifer, I, Muller-Karger, F, Solow, A, Silva, M and **Swayze, G.** 2015. Natural and unnatural oil slicks in the Gulf of Mexico. *J Geophys Res Ocean* **120**(12): 8364–8380. DOI: https://doi.org/10.1002/2015JC011062

Magen, C, Lapham, LL, Pohlman, JW, Marshall, K, Bosman, S, Casso, M and **Chanton, JP.** 2014. A simple headspace equilibration method for measuring dissolved methane. *Limnol Oceanogr: Methods* **12**: 637–650. DOI: https://doi.org/10.4319/lom.2014.12.637

McNichol, AP and **Aluwihare, LI.** 2007. The power of radiocarbon in biogeochemical studies of the marine carbon cycle: insights from studies of dissolved and particulate organic carbon (DOC and POC). *Chem Rev* **107**(2): 443–466. DOI: https://doi.org/10.1021/cr050374g

Montoya, JP, Horrigan, SG and **McCarthy, JJ.** 1990. Natural abundance of ^{15}N in particulate nitrogen and zooplankton in the Chesapeake Bay. *Mar Ecol Prog Ser* **65**: 35–61. DOI: https://doi.org/10.3354/meps065035

Peterson, B, Fry, B, Hullar, M, Saupe, S and **Wright, R.** 1994. The distribution and stable carbon isotopic composition of dissolved organic carbon in estuaries. *Estuaries* **17**(1B): 111–121. DOI: https://doi.org/10.2307/1352560

Rakowski, C, Magen, C, Bosman, S, Rogers, KL, Gillies, LE, Chanton, JP and **Mason, OU.** 2015. Methane and microbial dynamics in the Gulf of Mexico water column. *Front Mar Sci* **2**: 69. DOI: https://doi.org/10.3389/fmars.2015.00069

R Core Team. 2015. R: A language and environment for statistical computing. Vienna, Austria: R Foundation for Statistical Computing. Available at http://www.R-project.org/.

Skarke, A, Ruppel, C, Kodis, M, Brothers, D and **Lobecker, E.** 2014. Widespread methane leakage from the sea floor on the northern US Atlantic margin. *Nat Geosci* **7**: 657–661. DOI: https://doi.org/10.1038/ngeo2232

Stock, BC and **Semmens, BX.** 2016. MixSIAR GUI User Manual. Version 3.1. https://github.com/brianstock/MixSIAR. DOI: https://doi.org/10.5281/zenodo.47719

Stuiver, M and **Pollach, HA.** 1977. Discussion: Reporting of ^{14}C data. *Radiocarbon* **19**(3): 355–363. PDF, University of Arizona, 1999. DOI: https://doi.org/10.1017/S0033822200003672

Tazaz, AM, Bebout, BM, Kelley, CA, Poole, J and **Chanton, JP.** 2013. Redefining the isotopic boundaries of biogenic methane: Methane from endoevaporites. *Icarus* **224**(2): 268–275. DOI: https://doi.org/10.1016/j.icarus.2012.06.008

Valentine, DL, Kessler, JD, Redmond, MC, Mendes, SD, Heintz, MB, Farwell, C, Hu, L, Kinnaman, FS, Yvon-Lewis, S, Du, M, Chan, EW, Garcia Tigreros, F and **Villanueva, CJ.** 2010. Propane respiration jump-starts microbial response to a deep oil spill. *Science* **330**(6001): 208–211. DOI: https://doi.org/10.1126/science.1196830

Walker, BD, Druffel, ERM, Kolasinski, J, Roberts, BJ, Xu, X and **Rosenheim, BE.** 2017. Stable and radiocarbon isotopic composition of dissolved organic matter in the Gulf of Mexico. *Geophys Res Lett* **44**: 8424–8434. DOI: https://doi.org/10.1002/2017GL074155

Wang, X-C, Chen, RF and **Gardner, GB.** 2004. Sources and transport of dissolved and particulate organic carbon in the Mississippi River estuary and adjacent coastal waters of the northern Gulf of Mexico. *Mar Chem* **89**: 241–256. DOI: https://doi.org/10.1016/j.marchem.2004.02.014

Weber, SC, Peterson, L, Battles, JJ, Roberts, BJ, Peterson, RN, Hollander, DJ, Chanton, JP, Joye,

SB and **Montoya, JP.** 2016. Hercules 265 rapid response: Immediate ecosystem impacts of a natural gas blowout incident. *Deep-Sea Res Pt II* **129**: 66–76. DOI: https://doi.org/10.1016/j.dsr2.2015.11.010

Williams, PM and **Druffel, ERM.** 1987. Radiocarbon in dissolved organic matter in the central North Pacific Ocean. *Nature* **330**: 246–248. DOI: https://doi.org/10.1038/330246a0

Wilson, RM, Cherrier, J, Sarkodee-Adoo, J, Bosman, S, Mickle, A and **Chanton, JP.** 2016. Tracing the intrusion of fossil carbon into coastal Louisiana macrofauna using natural ^{14}C and ^{13}C abundances.

Deep Sea Res Pt II **129**: 89–95. DOI: https://doi.org/10.1016/j.dsr2.2015.05.014

Yan, B, Passow, U, Chanton, JP, Nöthig, E-M, Asper, V, Sweet, J, Pitiranggon, M, Diercks, A and **Pak, D.** 2016. Sustained deposition of contaminants from the Deepwater Horizon spill. *Proc Natl Acad Sci USA* **113**(24): E3332–E3340. DOI: https://doi.org/10.1073/pnas.1513156113

Yvon-Lewis, SA, Hu, L and **Kessler, J.** 2011. Methane flux to the atmosphere from the Deepwater Horizon oil disaster. *Geophys Res Lett* **38**: L01602. DOI: https://doi.org/10.1029/2010GL045928